# A Capacitive-Coupling Winding Tap Injection DSTATCOM Integrated with Distribution Transformer for Balance and Unbalance Operations

Ziyi Bai, Ying Pang, *Student Member*, *IEEE*, Zeng Xiang, *Member*, *IEEE*, Chi-Kong Wong, *Member*, *IEEE*, Lei Wang, *Senior Member*, *IEEE,* Chi-Seng Lam, *Senior Member*, *IEEE*, Man-Chung Wong, *Senior Member*, *IEEE*

***Abstract*—The intelligent substations should be developed to perform multifunction operations, including power flow control, voltage regulation, and cost-effective power quality improvement. In this paper, an intelligent substation by a distribution transformer integrated with a capacitive-coupling winding tap injection static synchronous compensator (CWTI-DSTATCOM) is proposed for balance and unbalance operations. Compared with the state-of-the-art approaches, CWTI-DSTATCOM can operate at a low dc voltage with a small active inverter rating, which also can provide distributed voltage, reactive, and unbalanced current compensation. The power rating reduction mechanism is mathematically revealed via balance and unbalance compensation analysis, which is further used to determine the optimal inverter power rating of unbalance operation via an optimal *LC* filter design method. Furthermore, a comprehensive compensation control strategy is developed to coordinate the transformer taps and the active inverter under balanced and unbalanced operations. Simulation and real-time digital simulator (RTDS) hardware-in-the-loop (HIL) experiments are performed to prove the validity and effectiveness of the proposed topology over inverter rating reduction and power quality enhancement.**

***Index Terms*—static synchronous compensator (STATCOM), unbalanced compensation, winding tap, *LC* filter, symmetry sequence, power rating.**

Manuscript received September 05, 2021; revised January 18, 2022; accepted February 18, 2022. This work was supported by Macau Science and Technology Development Fund (FDCT, Macao) under Projects FDCT 0026/2019/A1, in part by the State Key Laboratory of Internet of Things of University of Macau under Project SKL-IOTSC(UM)-2021-2023, in part by the Guangdong-Hong Kong-Macau Joint Laboratory for Smart Cities under Project EF008/IOTSC-YKV/2021/GDSTC, in part by Research Committee of University of Macau under project MYRG2018-00056-FST, and in part by the Hunan Youth Science and Technology Innovation Talents Program under Project 2021RC3059. *(Corresponding author: Lei Wang; Man-Chung Wong.)*

Ziyi Bai, Ying Pang, Zeng Xiang, and Chi-Kong Wong are with the State Key Laboratory of Internet of Things for Smart City, University of Macau, Macao 999078, China, also with the Department of Electrical and Computer Engineering, Faculty of Science and Technology, University of Macau, Macao 999078, China (e-mail: yc07909@um.edu.mo; yb87446@um.edu.mo; yb57435@umac.mo; ckwong@um.edu.mo).

Lei Wang is with the College of Electrical and Information Engineering, Hunan University, Changsha 410000, China (email: jordanwanglei@hnu.edu.cn).

Chi-Seng Lam is with the State Key Laboratory of Analog and Mixed-Signal VLSI, University of Macau, Macao 999078, China, also with the Institute of Microelectronics, University of Macau, Macao 999078, China, and also with the Department of Electrical and Computer Engineering, Faculty of Science and Technology, University of Macau, Macao 999078, China. (e-mail: cslam@um.edu.mo)

Man-Chung Wong is with the State Key Laboratory of Internet of Things for Smart City, University of Macau, Macao 999078, China, and also with the State Key Laboratory of Analog and Mixed-Signal VLSI, University of Macau, Macao 999078, China, and also with the Department of Electrical and Computer Engineering, Faculty of Science and Technology, University of Macau, Macao 999078, China (e-mail: mcwong@umac.mo).

## I. Introduction

In present distribution systems, unbalanced nonlinear loads in three-phase utility have given rise to a number of power quality (PQ) problems, such as low power factor (PF), harmonic pollution, and unbalanced currents. Excessive reactive power demand increases feeder losses and reduces active power transfer capability, whereas the unbalance current endangers the safe operation of transformers and generators [1], [2]. Due to their fast dynamic response and excellent compensation performance, distribution static synchronous compensators (DSTATCOMs) [3], [4] have been widely used to provide reactive power and unbalance compensation and improve the PQ of the network.

In order to improve the PQ, DSTATCOMs are installed locally at the customer-side to maintain the local bus voltage [5], [6]. Local compensations at some light-load buses are unable to share their excess capacity to other heavy-load buses [7]. As a result, a large number of decentralized STATCOMs need to be installed, which increases the total investment and maintenance costs. Recently intelligent box-type substations [8] and centralized compensation systems [7] for low voltage distribution networks are proposed to address the above high-cost issues. The integration of distribution transformer and power quality compensator can achieve multifunction operations, such as distributed voltage regulation and power flow control, which turns to become more and more important to accelerate the smart grid development.

Conventionally, intelligent box-type substations equipped with DSTATCOM [8] have promising application prospects in the distribution systems due to their compact design, small floor space, and flexible installed environment. The centralized compensation system can be easily expanded to meet future load growth [7]. There are two usual installed positions of DSTATCOMs, including the low-voltage (LV) and high-voltage (HV) sides of the transformer. While the larger DSTATCOM current level for the LV side installation would result in high heating and power losses of the devices, the DSTATCOM current level for the HV side installation is lower.

Fig. 1 summarized the historical development, circuit configurations, proposed years, and corresponding references for different topologies which integrate the STATCOM with the high voltage side of a distribution transformer. As shown in Fig. 1 (a), the *Topology 1* [9] was proposed in 1981, and its D-STATCOM is connected to the HV side of a distributed transformer through a step-down transformer. Further studies relating to its structure, features, and applications were

This article has been accepted for publication in a future issue of this journal, but has not been fully edited. Content may change prior to final publication. Citation information: DOI 10.1109/TIE.2022.3156042, IEEE Transactions on Industrial Electronics



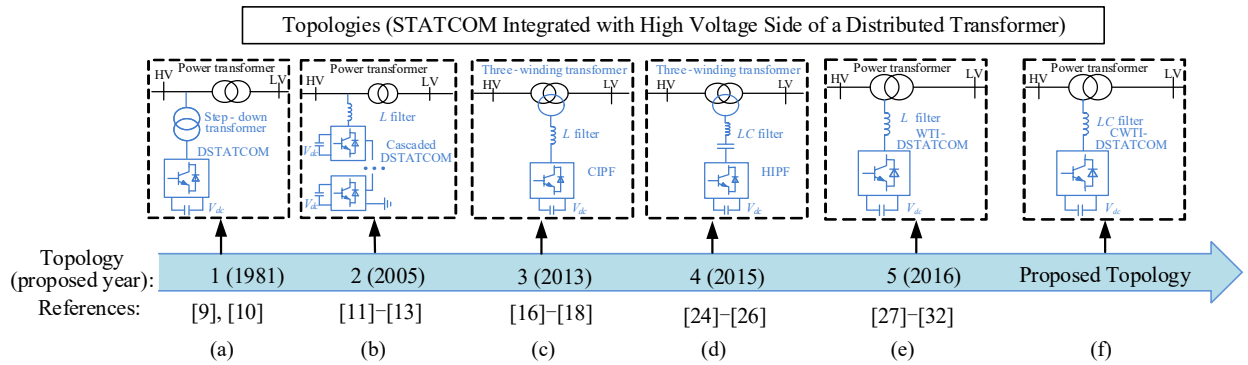


Fig. 1. DSTATCOM connection type comparison of: (a) *Topology 1*, (b) *Topology 2*, (c) *Topology 3*, (d) *Topology 4*, (e) *Topology 5*, and (f) proposed capacitive DSTATCOM integrated with transformer taps.

addressed in [10] in 2014. In 2005, cascaded multilevel DSTATCOM, as *Topology 2* shown in Fig. 1 (b) [11], was proposed to connect directly to the grid instead. The multilevel structure needs relatively more power electronic components and dc-linked capacitors [12], which will cause more power switching loss, economic and reliability issues [13]. On the other hand, the multilevel structure requires more pulses and drivers to control the system so that a complicated controller is required [12].

Based on the above concerns for multilevel structure, a STATCOM integrated with the distribution transformer is researched, which is a cost-effective centralized power quality compensation method to improve the PQ [6], [14], [15]. As a result, controllably inductive power filters (CIPF), which is a three-winding transformer structure was proposed in 2013 as *Topology 3* [16]–[20] shown in Fig. 1 (c). Its operation mechanism and control strategy were studied in [16]–[18]. Such topology was further applied into non-linear load scenarios [19] in 2013 and photovoltaic power plants [20] in 2019, respectively. Compared with the *L*-coupling inverter, the *LC*-coupling inverter can reduce the voltage source inverter (VSI) rating and dc-link voltage [21]–[23]. Thus, hybrid inductive and active filter (HIAF), *as Topology 4* shown in Fig. 1 (d), was proposed in 2015 in [24] by replacing the *L* filter with *LC* filter. After that, *Topology 4* was applied in shipboard [25] in 2017 and DC grid applications [26] accordingly in 2020.

Based on the cost reduction concern and motivated by the structure of autotransformer, the STATCOM was directly connected with the distribution transformer via winding taps instead of an auxiliary step-down transformer in 2016 [27]–[29], which were applied to traction power system. After that, [30] proposed a winding tap injection DSTATCOM (WTI-DSTATCOM) integrated with a distribution transformer in 2018, as *Topology 5* shown in Fig. 1 (e). Its operation mechanism and model analysis were studied in [30], and the advanced control strategies were analyzed in [31]–[32] respectively between 2018 and 2020. For the inverter rating reduction of the conventional WTI-DSTATCOM [27]–[32], this paper proposes a centralized compensation topology and control strategy of capacitive-coupling winding tap injection-based DSTATCOM (CWTI-DSTATCOM) as shown in Fig. 1 (f).

A comparison among different topologies is summarized in Table I. Through the additional step-down transformer,

TABLE I
COMPARISONS OF TOPOLOGIES 1-5, AND PROPOSED TOPOLOGY

| Topology | Windings customized | DC-link voltage | Inverter rating | Unbalance operation | Cost | Structure |
|---|---|---|---|---|---|---|
| 1 [9]-[10] | No | Medium | High | Yes | High | Simple |
| 2 [11]-[13]] | No | Low | High | Yes | High | Complex |
| 3 [16]-[18] | Yes | Medium | High | Yes | High | Complex |
| 4 [24]-[26] | Yes | Low | Low | Yes | High | Complex |
| 5 [27]-[32] | No | High | High | No | Medium | Simple |
| Proposed | No | Low | Low | Yes | Low | Simple |

*Note*: the unsatisfying characteristics are shaded.

relatively medium dc-link voltage and higher inverter rating of *Topology 1* are required so that its initial cost is increased. The multilevel structure of *Topology 2* decreases the dc-link voltage of each inverter and however the more power electronic components increase its cost and structural complexity. Though *Topologies 3 and 4* can reduce the dc-link voltage, the induction filter windings and transformers must be customized. Since the active inverter bears all the compensation power, high inverter ratings are required for *Topologies 1-3*, whereas the inverter rating of *Topology 4* can be lower due to its *LC* filters. As the medium cost and simple structure, more attention on *Topology 5* was obtained recently. However, both the VSI rating and dc-link voltage of *Topology 5* are relatively higher comparing to the proposed one. Its unbalanced operation and transformer tap ratio to converter rating have not been addressed yet.

In the proposed topology, the VSI of CWTI-DSTATCOM is connected to the adjustable transformer primary winding taps via a capacitive *LC* part. The capacitive *LC* part provides a high voltage drop between the tap coupling point and the active inverter so that the inverter can work at a lower dc-link voltage level relatively. The capacitive *LC* also offers a certain reactive power to reduce the required inverter rating through designing the parameters technically. In such case, only a low-rating active inverter is required to absorb the residual balanced and unbalanced power. The contributions of this paper are summarized as follows.

1) A CWTI-DSTATCOM is proposed to integrate STATCOM with tapped transformer by coupling *LC* filters. The following technical issues are studied:

- Reduction of power ratings comparing with existing solution WTI-DSTATCOM under balanced and unbalanced situations;
- Influence of component parameters including the transformer winding tap ratio and coupling impedance to the inverter rating;

- The minimum dc-link voltage of DSTATCOM for acceptable performance and low operational loss under balanced and unbalanced situations;
- Cost comparison between existing solution WTI-DSTATCOM and the proposed one.

2) Comparing to existing WTI-DSTATCOM, the inverter rating of CWTI-DSTATCOM is only 12% and 33% of WTI-DSTATCOM under balanced and 30% unbalanced cases, respectively.

3) The transformer winding tap ratio is firstly studied to reduce the required rating of DSTATCOM, and the tap ratio should be 0.5 for the minimum DSTATCOM rating.

4) The strategy of computing its minimum dc-link voltage is proposed based on the symmetrical component theory.

5) Corresponding control is given with considering transformer taps and sufficient dc-link voltage.

## II. Circuit Configuration and Modeling of the Proposed CWTI-STATCOM

### A. Circuit Configuration

Fig. 2 gives the circuit configuration of the proposed CWTI-DSTATCOM, which includes a passive part and an active inverter part connected to the transformer winding taps points. Here, the subscript "$x$" denotes phase $x = a, b, c$. $v_{Sx}$, $v_{Lx}$, $v_{cx}$, $i_{Sx}$, $i_{Lx}$, $i_{cx}$ represent the source voltage, the load voltage, the winding tap coupling point voltage, the source

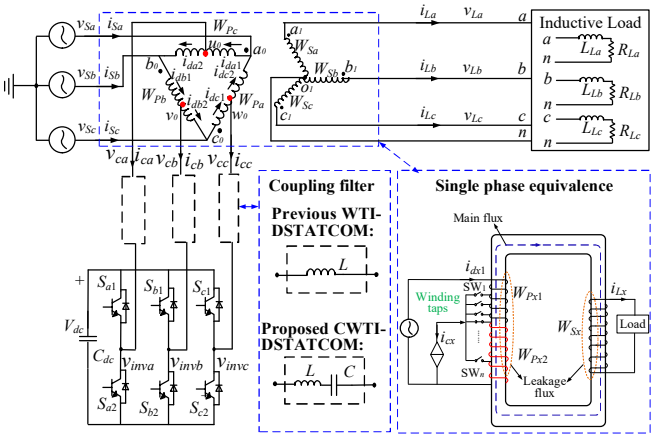


Fig. 2. Circuit configuration of the proposed CWTI-DSTATCOM and previous WTI-DSTATCOM.

current, the load current, the compensation current, respectively. $C_{dc}$ and $V_{dc}$ are the DC capacitor and dc-link voltage. The inverter is connected to the adjustable taps (labeled as $u_0$, $v_0$, and $w_0$) on primary winding (labeled as $a_0$-$b_0$, $b_0$-$c_0$, and $c_0$-$a_0$) of the transformer through coupling inductor $L$ and capacitor $C$. $L_{Lx}$ and $R_{Lx}$ are the load inductance and resistance, respectively. $W_{Px}$ (primary side) and $W_{Sx}$ (secondary side) denote the winding turns of Dyn11 connected distribution transformer. The winding turns on both sides of the taps are $W_{Px1}$ and $W_{Px2}$ ($W_{Px1}$+$W_{Px2}$=$W_{Px}$). $i_{dx}$ is delta-loop connected windings currents. The SW$_n$ represents the switches used to select the taps.

### B. Current Modeling

Based on the Kirchhoff's current law and ampere-turns balance principle of the distribution transformer, the relationship among source current, load current, and compensation current in Fig. 2 is shown as,

$$\begin{bmatrix} i_{Sa} \\ i_{Sb} \\ i_{Sc} \end{bmatrix} = M \cdot \begin{bmatrix} i_{La} \\ i_{Lb} \\ i_{Lc} \end{bmatrix} + N \cdot \begin{bmatrix} i_{ca} \\ i_{cb} \\ i_{cc} \end{bmatrix} \tag{1}$$

where the transform matrix $M$ and $N$ are shown as,

$$M = \begin{bmatrix} \frac{W_{Sa}}{W_{Pa}} & 0 & -\frac{W_{Sc}}{W_{Pc}} \\ -\frac{W_{Sa}}{W_{Pa}} & \frac{W_{Sb}}{W_{Pb}} & 0 \\ 0 & -\frac{W_{Sb}}{W_{Pb}} & \frac{W_{Sc}}{W_{Pc}} \end{bmatrix} = \frac{1}{K_x}\begin{bmatrix} 1 & 0 & -1 \\ -1 & 1 & 0 \\ 0 & -1 & 1 \end{bmatrix} \tag{2}$$

$$N = \begin{bmatrix} \frac{W_{Pa2}}{W_{Pa}} & 0 & \frac{W_{Pc1}}{W_{Pc}} \\ \frac{W_{Pa1}}{W_{Pa}} & \frac{W_{Pb2}}{W_{Pb}} & 0 \\ 0 & \frac{W_{Pb1}}{W_{Pb}} & \frac{W_{Pc2}}{W_{Pc}} \end{bmatrix} = \begin{bmatrix} 1-k_x & 0 & k_x \\ k_x & 1-k_x & 0 \\ 0 & k_x & 1-k_x \end{bmatrix} \tag{3}$$

In (2) and (3), $K_x = W_{Sx}/W_{Px}$ is the turn ratio of the transformer and $K_a = K_b = K_c$. Here, the turn ratio $K$ is larger than 1 as a result of the step-down transformer. $k_x$ represents the winding tap ratio. $k_x = W_{Px1}/W_{Px}$ and $k_a = k_b = k_c$. When the compensation current $i_{cx}$ satisfy (4), only the active current exists in the source current $i_{Sx}$.

$$\begin{bmatrix} i_{ca} \\ i_{cb} \\ i_{cc} \end{bmatrix} = -N^{-1} \cdot M \cdot \begin{bmatrix} i_{La} - i_{Lap} \\ i_{Lb} - i_{Lbp} \\ i_{Lc} - i_{Lcp} \end{bmatrix} \tag{4}$$

The $i_{Lxp}$ in (4) is the active component of the load current. The load current in 0-1-2 coordinate can be calculated by applying symmetrical component theory as,

$$\begin{bmatrix} I_{L0}\angle\theta_{IL0} \\ I_{L1}\angle\theta_{IL1} \\ I_{L2}\angle\theta_{IL2} \end{bmatrix} = A \cdot \begin{bmatrix} I_{La}\angle\theta_{ILa} \\ I_{Lb}\angle\theta_{ILb} \\ I_{Lc}\angle\theta_{ILc} \end{bmatrix} \tag{5}$$

where

$$A = \frac{1}{3}\begin{bmatrix} 1 & 1 & 1 \\ 1 & a & a^2 \\ 1 & a^2 & a \end{bmatrix}, \text{ and } A^{-1} = \begin{bmatrix} 1 & 1 & 1 \\ 1 & a^2 & a \\ 1 & a & a^2 \end{bmatrix} \tag{6}$$

In (6), $a = e^{j120^\circ}$. The phasor magnitude of the load current $I_{Lx}$ and angle $\theta_{ILx}$ can be obtained by using (7)–(9). Noted that the 0-1-2 coordinate is adopted as the basic framework in this paper for balance and unbalance operations, while the dq0 framework in (7)-(9) is adopted to calculate the load current $I_{Lx}$ and angle $\theta_{ILx}$. $i_{Lx}^D$ is the $i_{Lx}$ signal delay by 90°. $\bar{i}_{Lxd}$ and $\bar{i}_{Lxq}$ are the dc components of the d-axis component $i_{Lxd}$ and q-axis component $i_{Lxq}$. $\omega t$ is the input angle of $dq$ transformation.

$$\begin{bmatrix} i_{Lxd} \\ i_{Lxq} \end{bmatrix} = \begin{bmatrix} \cos\omega t & \sin\omega t \\ -\sin\omega t & \cos\omega t \end{bmatrix}\begin{bmatrix} i_{Lx} \\ i_{Lx}^D \end{bmatrix} \tag{7}$$

$$I_{Lx} = \sqrt{\bar{i}_{Lxd}^{\,2} + \bar{i}_{Lxq}^{\,2}} \tag{8}$$

$$\theta_{ILx} = \arctan\left(\bar{i}_{Lxq} / \bar{i}_{Lxd}\right) \tag{9}$$

For the CWTI-DSTATCOM, based on (4)–(6), the compensation current in 0-1-2 coordinate can be deduced as,

$$\begin{bmatrix} I_{c0}\angle\theta_{Ic0} \\ I_{c1}\angle\theta_{Ic1} \\ I_{c2}\angle\theta_{Ic2} \end{bmatrix} = -A \cdot N^{-1} \cdot M \cdot A^{-1} \cdot \begin{bmatrix} 0 \\ I_{L1}\sin\theta_{IL1}\angle 90^\circ \\ I_{L2}\angle\theta_{IL2} \end{bmatrix} \tag{10}$$

where $I_{L1}\sin\theta_{IL1}$ is the loading fundamental reactive current in 1-sequence. Due to the delta-connected primary windings of the transformer, the 0-sequence component is zero.

### C. Voltage Modeling

The primary side voltage vector diagram of the delta-star connected transformer is given in Fig. 3 (a), in which $o_0$ is the virtual neutral point. The winding turns ratio on both sides of the tap coupling points is $k_x$ :1–$k_x$. Based on, the $v_{cx}$ can be deduced as,

$$v_{cx} = \frac{u_0 v_0}{a_0 b_0} v_{Sx} = \sqrt{3k_x^2 - 3k_x + 1} \cdot v_{Sx} \tag{11}$$

Based on (11), Fig. 3 (b) shows the relationship of the winding tap ratio and tap coupling point voltage when the grid line-to-line voltage is 10kV. It clearly shows that the minimum coupling point voltage is $0.5V_S$ when $k_x = 0.5$, i.e., the center taps are chosen to connect the VSI. The minimum coupling point voltage reflects the minimum required VSI dc-link voltage and rating.

Then, the tap coupling point voltage $V_{c012}$ in 0-1-2 coordinate can be computed as,

$$V_{c012} = A \cdot V_{cabc} \tag{12}$$

Fig. 4 (a) and (b) show the a-b-c and 0-1-2 circuit models of the CWTI-STATCOM between the coupling point and the active inverter part, respectively. The coupling impedance in 0-1-2 coordinate can be deduced as,

$$X_{012} = A X_{abc} A^{-1} = \begin{bmatrix} X & 0 & 0 \\ 0 & X & 0 \\ 0 & 0 & X \end{bmatrix} = X_{abc} \tag{13}$$

where $X_{abc}$ and $X_{012}$ are the coupling impedances in a-b-c and 0-1-2 coordinates. The $X$ represents the coupling filter impedance, which can be expressed as (14) for the WTI-DSTATCOM or (15) for CWTI-DSTATCOM.

$$X = X_L = j\omega L \tag{14}$$

$$X = X_{LC} = -j\left(\frac{1}{\omega C} - \omega L\right) \tag{15}$$

Based on the circuit model in 0-1-2 coordinate of Fig. 4, the inverter output voltage $V_{inv012}$ of the CWTI-DSTATCOM can be calculated as,

1-sequence
$$V_{inv1}\angle\theta_{V_{inv1}} = |V_{c1}|\angle 0^\circ - |X||I_{c1}|\angle\left(\theta_X + \theta_{I_{c1}}\right) \tag{16}$$

2-sequence
$$V_{inv2}\angle\theta_{V_{inv2}} = -|X||I_{c2}|\angle\left(\theta_X + \theta_{I_{c2}}\right) \tag{17}$$

where the $V_{c0}$ and $V_{c2}$ are zero due to the same tap ratios. $\theta_X$ represents the angle of the coupling impendence.

Based on (16)–(17), the inverter output voltages in a-b-c coordinate can be deduced as,

$$\begin{bmatrix} V_{inva}\angle\theta_{V_{inva}} \\ V_{invb}\angle\theta_{V_{invb}} \\ V_{invc}\angle\theta_{V_{invc}} \end{bmatrix} = A^{-1} \cdot \begin{bmatrix} 0 \\ V_{inv1}\angle\theta_{V_{inv1}} \\ V_{inv2}\angle\theta_{V_{inv2}} \end{bmatrix} \tag{18}$$

Assume the modulation index $m$ is $m$=1, the required dc-link voltage $V_{dc}$ is designed to the line-to-line peak value of the maximum inverter voltage $V_{invmax}$ in a-b-c coordinate. It can be formulated as,

$$V_{invmax} = \max(V_{inva}, V_{invb}, V_{invc}) \tag{19}$$

$$V_{dc} = \sqrt{3}V_{invmax} \tag{20}$$

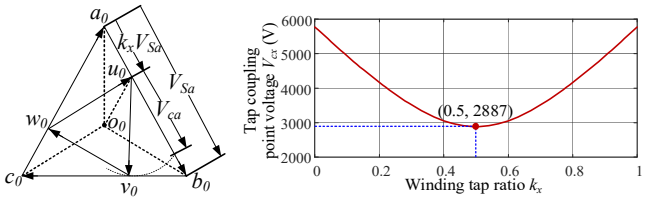


Fig. 3. (a) Primary-side voltage vector diagram; (b) relationship between tap ratio and tap coupling point voltage of the distributed transformer.

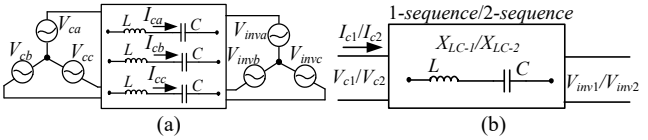


Fig. 4. Circuit of the CWTI-STATCOM in (a) a-b-c; (b) 0-1-2 coordinates.

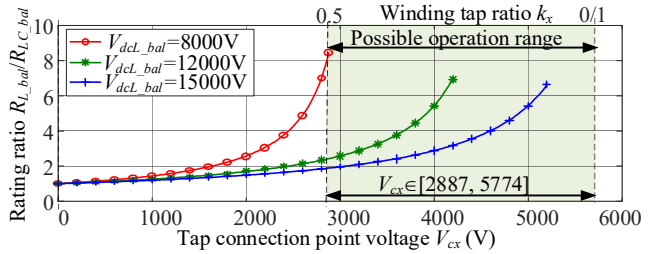


Fig. 5. Ratio $R_{L\_bal}/R_{LC\_bal}$ in terms of $V_{cx}$ and $V_{dcL\_bal}$.

### D. Rating Modeling

For the CWTI-DSTATCOM, the impedance $X_C$ of the capacitor is much higher than $X_L$ of the inductor as shown in (21). Thus the overall $LC$-coupling impedance $X_{LC}$ in (15) is still capacitive.

$$|X_C| >> |X_L| \tag{21}$$

The VSI power rating ratio analyses of the WTI-DSTATCOM and CWTI-DSTATCOM under balanced and unbalanced load are given in the following.

#### a) Balanced Load

For balanced load, the compensation current and inverter output voltage contain only the 1-sequence component. Thus, the required VSI power rating ratio between the WTI-DSTATCOM and CWTI-DSTATCOM can be expressed as,

$$\frac{R_{L\_bal}}{R_{LC\_bal}} = \frac{V_{invL\_bal} \cdot I_{c1}}{V_{invLC\_bal} \cdot I_{c1}} = \frac{V_{dcL\_bal} \cdot I_{c1}}{V_{dcLC\_bal} \cdot I_{c1}} = \frac{V_{dcL\_bal}}{V_{dcLC\_bal}} \tag{22}$$

According to [33], the equivalent current to link up dc-link voltages between the $L$- and $LC$- coupling inverters under balanced load case can be expressed as (23). The (23) holds if the $L$ value is the same for both coupling $L$ and $LC$ filter, the initial voltage value of the coupling capacitor is almost equal to $v_{cx}$, and the initial value of $i_{cx}$ is assumed to be zero. Based on (23), the VSI power rating ratio in (22) can be further deduced as (24).

$$V_{dcLC\_bal} = V_{dcL\_bal} - \sqrt{6}V_{cx} \tag{23}$$

$$\frac{R_{L\_bal}}{R_{LC\_bal}} = \left(1 + \frac{\sqrt{6}V_{cx}}{V_{dcL\_bal} - \sqrt{6}V_{cx}}\right) \tag{24}$$

According to (24), the required VSI power rating of the CWTI-DSTATCOM is always less than that of WTI-DSTATCOM due to $V_{dcL\_bal} > \sqrt{6}V_{cx}$ as (23). Fig. 5 shows the relationship between $R_{L\_bal}/R_{LC\_bal}$ and $V_{cx}$ under different $V_{dcL\_bal}$. The $V_{dcL\_bal}$= 8000V and $V_{dcLC\_bal}$ = 930V are chosen that touches the $V_{cx}$= 2887V at $k_x$ = 0.5 in the possible operation range ($V_{cx}$∈[2887, 5774]), yielding the maximum rating ratio $R_{L\_bal}/R_{LC\_bal}$ = 8.6.

From the above VSI rating discussion under balanced loads, two important points can be summarized as follows:

- When the source grid voltage $V_{sx}$ is given, the winding tap ratio $k_x$ can be chosen at 0.5 so that its coupling point voltage $V_{cx}$ can be smaller.
- The $V_{dcLC\_bal}$ and $R_{LC\_bal}$ of the CWTI-DSTATCOM are always smaller than WTI-DSTATCOM.

*b) Unbalanced Load*

For unbalanced load, the compensation current includes 1- and 2-sequence components. Assume that the unbalance coefficient $\varepsilon$ is defined as the 2-sequence current amplitude divided by the 1-sequence one,

$$\varepsilon = \frac{I_{c2}}{I_{c1}} \tag{25}$$

The maximum compensation current can be treated as the amplitude sum of $I_{c1}$ and $I_{c2}$ when considering the worst case. The inverter output voltage includes 1- and 2-sequence voltages in (16) and (17). Similarly, the maximum inverter output voltage can also be treated as the amplitude sum of $V_{inv1}$ and $V_{inv2}$. Considering the worst case under unbalanced load, the required VSI power rating ratio between unbalanced and balanced load can be formulated as,

$$\frac{R_{unbal}}{R_{bal}} = \frac{V_{dc\_unbal} \cdot (I_{c1} + I_{c2})}{V_{dc\_bal} \cdot I_{c1}} \tag{26}$$

where the required dc-link voltage ratio between the worst unbalanced and balanced conditions can be expressed as (27) based on (14)–(17), and (25).

$$\begin{aligned} \frac{V_{dcL/LC\_unbal}}{V_{dcL/LC\_bal}} &= \frac{V_{inv1} + V_{inv2}}{V_{inv1}} = \frac{V_{inv1} + \varepsilon(\pm V_{inv1} \mp V_{cx})}{V_{inv1}} \\ &= \frac{(1 \pm \varepsilon)V_{dc\_bal} \mp \sqrt{6}\varepsilon V_{cx}}{V_{dc\_bal}} \end{aligned} \tag{27}$$

Based on the above analysis, for the WTI-DSTATCOM and CWTI-DSTATCOM, the required VSI power rating ratios between the unbalanced and balanced conditions can be further deduced as,

$$\frac{R_{L\_unbal}}{R_{L\_bal}} = (1+\varepsilon)\frac{(1+\varepsilon)V_{dcL\_bal} - \sqrt{6}\varepsilon V_{cx}}{V_{dcL\_bal}} \tag{28}$$

$$\frac{R_{LC\_unbal}}{R_{LC\_bal}} = (1+\varepsilon)\frac{(1-\varepsilon)V_{dcLC\_bal} + \sqrt{6}\varepsilon V_{cx}}{V_{dcLC\_bal}} \tag{29}$$

Based on (28) and (29), when the 2-sequence compensation current is required, the required VSI power ratings of WTI-DSTATCOM and CWTI-DSTATCOM increase due to the $V_{dcL\_bal} > \sqrt{6}V_{cx}$ and $V_{dcLC\_bal} < \sqrt{6}V_{cx}$. The required VSI power rating ratio between the CWTI-DSTATCOM and WTI-DSTATCOM can be expressed as,

$$\frac{R_{LC\_unbal}}{R_{L\_unbal}} = \frac{(1-\varepsilon)V_{dcLC\_bal} + \sqrt{6}\varepsilon V_{cx}}{(1+\varepsilon)V_{dcL\_bal} - \sqrt{6}\varepsilon V_{cx}} \tag{30}$$

The VSI power rating ratios of $R_{L\_unbal}/R_{L\_bal}$, $R_{LC\_unbal}/R_{L\_bal}$, and $R_{LC\text{-}unbal}/R_{LC\text{-}bal}$ in terms of unbalance coefficient $\varepsilon$ are shown in Fig. 6 and 7. Taking $R_{L\_bal}$ as the base value, Fig. 6 shows that the required VSI ratings comparison for unbalanced cases. It implies that when the unbalance coefficient from 0 to 1.33, the required VSI dc-link voltage and rating of CWTI-DSTATCOM are lower than these of WTI-DSTATCOM. However, when the unbalance coefficient is larger than 1.33, the WTI-DSTATCOM is lower. On the other hand, taking $R_{LC\_bal}$ as the base value, Fig. 7 shows the required power rating ratio between unbalance case and balance case for the CWTI-DSTATCOM.

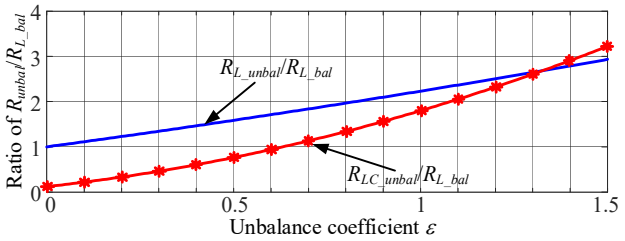


Fig. 6. Ratios $R_{L\_unbal}/R_{L\_bal}$ and $R_{LC\_unbal}/R_{L\_bal}$ in terms of $\varepsilon$.

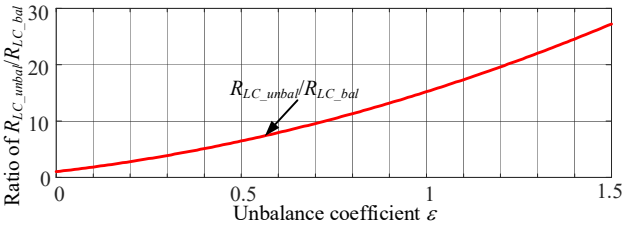


Fig. 7. Ratio of $R_{LC\_unbal}/R_{LC\_bal}$ in terms of $\varepsilon$.

From the above VSI power rating comparisons, several important points can be summarized as follows:

- When the load is balanced, the CWTI-DSTATCOM has a lower dc voltage and inverter rating compared with the conventional WTI-DSTATCOM, and it is only 12% inverter rating of the WTI-DSTATCOM.
- The required inverter rating is increased with the increase of the unbalance coefficient.
- When the unbalanced compensating current becomes larger, the CWTI-DSTATCOM is still preferable due to its lower rating. When the unbalance compensating current is less than 133% of the balanced one, the $V_{dcLC\_unbal}$ and $R_{LC\_unbal}$ of the CWTI-DSTATCOM are lower than those of WTI-DSTATCOM.

## III. Parameter Design and Power Rating Comparison

The selection of coupling parameters such as the inductance and capacitance of CWTI-DSTATCOM can affect the required dc-link voltage and rating. In this section, a conventional *LC* design method is given in the following part A for balanced load, whereas an optimal *LC* design method for unbalanced load is proposed in the following part B to further decrease the required dc-link voltage and inverter rating.

### *A. LC Design Based on Balanced Load*

The coupling $L$ is dedicated to filter out the current ripple brought by the power switches of the active inverter part [23]. Its value can be limited as (31),

$$L \geq \frac{V_{dc}}{8 f_s \cdot \Delta i_{c\max}} \tag{31}$$

where $f_s$ is the switching frequency and $\Delta i_{cmax}$ is the maximum allowed output ripple current.

Since the $I_{cx}$ is a fixed value under full compensation for a certain load, the minimum dc-link voltage $V_{dcLC\_min}$ indicates the minimum VSI power rating according to Section II-D. Thus, the required minimum dc-link voltage is the key point in designing the coupling *LC* impedance.

For balanced load, the *LC* impedance is selected conventionally to cope with the 1-sequence reactive current, thereby minimizing the inverter output voltage in 1-sequence to achieve low dc-link voltage design [23]. Thus, according

to (16), the coupling capacitance $C$=$C_{bal}$ based on balanced load is computed as,

$$C_{bal} = \frac{1}{2\pi f\left(\frac{V_{c1}}{I_{c1}} + 2\pi fL\right)} \tag{32}$$

### B. LC Design Based on Unbalanced Load

The *LC* design for balance operation only considers the 1-sequence component. To achieve the minimum dc-link voltage for unbalanced load, an *LC* design is proposed considering all symmetrical components simultaneously.

While the coupling $L$ can be expressed by (31), the deduction steps of the optimal coupling $C_{unbal}$ value of the CWTI-DSTATCOM for unbalanced load is shown in Fig. 8 to obtain the required minimum dc-link voltage. Firstly, three initial conditions should be calculated in advance: 1) based on the loading situation, the required compensating current of STATCOM is computed for reactive and unbalanced currents compensation; 2) based on the STATCOM integrating into a distributed transformer, its winding tap ratio is analyzed to reduce the required inverter dc-link voltage, and the lowest tap coupling point voltage can be obtained at winding tap ratio 0.5; 3) the *LC* coupling impedance is taken to get the inverter's output voltage by taking 0-1-2 coordinate for unbalance analysis. Then, the output voltages on each phase can be computed, and adjusting the coupling capacitance value can further reduce the output voltage of the inverter for unbalanced operation. Finally, the maximum inverter output voltage from all phases is selected to secure the compensation ability by transferring ac into the equivalent dc-link voltage of the inverter. Based on the above flowchart in Fig. 8, Fig. 9 gives a numerical example of the relationship between $V_{dcLC}$ and $C$ when the coupling $L$ is 10mH, and the load condition is shown in Table II. The optimal capacitance $C_{unbal}$ can be selected by solving (33) when the required $V_{dcLC}$ achieves the minimum.

Point A in Fig. 9 shows that the required minimum dc-link voltage is 2700V when the coupling capacitance is designed as 25μF based on the conventional design method. However, point B shows that the required minimum dc-link voltage is 1950V when the coupling capacitance is selected as 30.6μF based on the proposed *LC* design. The results show that the inverter dc-link and rating are reduced by 27.8%. These detailed results are shown in Table III.

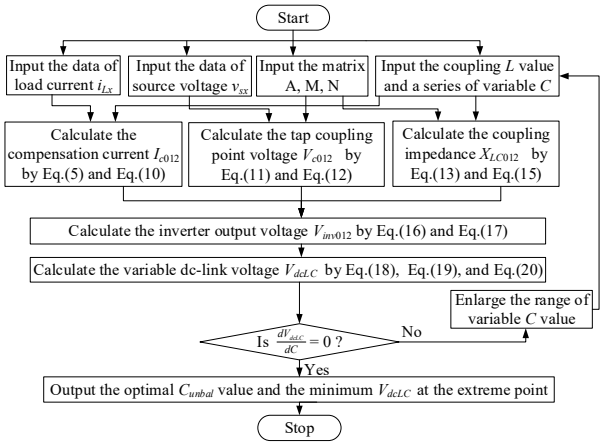


Fig. 8. Flowchart of the proposed $C_{unbal}$ design for unbalanced load.

TABLE II
UNBALANCED LOAD PARAMETERS WITH ε=0.3 WHEN $V_{SX}$=10KV, $K_X$ = 0.5

| a-b-c coordinate | | | 0-1-2 coordinate | | | |
|---|---|---|---|---|---|---|
| Phase | $I_L$ (A) | $I_S$ (A) (before comp.) | Sequence | $I_L$ (A) | $I_S$ (A) (before comp.) | $PF_{Lx}$ |
| A | 611.7∠-8.4 | 23.4∠-38.4 | 0 | 150∠-114.2 | 0 | 0.78 |
| B | 1054∠-122.4 | 31.2∠-145.7 | 1 | 758∠-5.6 | 28.9∠-35.6 | 0.85 |
| C | 611.7∠111.6 | 33∠76.9 | 2 | 150∠125.8 | 5.7∠155.7 | 0.78 |

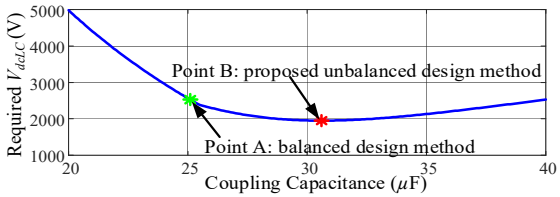


Fig. 9. Relationship between $V_{dcLC}$ and $C$ under the loading condition.

TABLE III
REQUIRED MINIMUM DC-LINK VOLTAGE COMPARISONS WITH DIFFERENT DESIGN METHODS

| Point | Coupling $L$ (mH) | Coupling $C$ (μF) | $V_{dc}$ (V) | $R_{LC}$ reduction (%) |
|---|---|---|---|---|
| A | 10 | 25.0 | 2700 | – |
| B | 10 | 30.6 | 1950 | 27.8 |

## IV. CONTROL SYSTEM OF CWTI-DSTATCOM

In this section, a comprehensive control strategy is proposed to coordinate the active inverter and the *LC* part of CWTI-DSTATCOM.

The load reactive, unbalanced, and harmonic power components are included in the reference compensating current $i_{cx}^*$. The inverter part is utilized to control the compensating current $i_{cx}$ to track its reference $i_{cx}^*$. The $i_{cx}^*$ can be deduced as,

$$\begin{bmatrix} i_{ca}^* \\ i_{cb}^* \\ i_{cc}^* \end{bmatrix} = \sqrt{\frac{2}{3}} \cdot \frac{1}{v_{c\alpha}^2 + v_{c\beta}^2} \begin{bmatrix} 1 & 0 \\ -1/2 & \sqrt{3}/2 \\ -1/2 & -\sqrt{3}/2 \end{bmatrix} \cdot \begin{bmatrix} v_{c\alpha} & -v_{c\beta} \\ v_{c\beta} & v_{c\alpha} \end{bmatrix} \cdot \begin{bmatrix} \tilde{p}_{\alpha\beta} + dc_p \\ \tilde{q}_{\alpha\beta} + \tilde{q}_{\alpha\beta} \end{bmatrix} \tag{34}$$

where the tap coupling point voltages ($v_{c\alpha}$ and $v_{c\beta}$) in the *α-β* plane can be transformed from *a-b–c* frames as,

$$\begin{bmatrix} v_{c\alpha} \\ v_{c\beta} \end{bmatrix} = \sqrt{\frac{2}{3}} \begin{bmatrix} 1 & -1/2 & -1/2 \\ 0 & \sqrt{3}/2 & -\sqrt{3}/2 \end{bmatrix} \cdot \begin{bmatrix} v_{ca} \\ v_{cb} \\ v_{cc} \end{bmatrix} \tag{35}$$

where $v_{cx}$ can be calculated based on the (11) and transformer ratio $K$. It can be formulated as,

$$\begin{bmatrix} v_{ca} \\ v_{cb} \\ v_{cc} \end{bmatrix} = K \cdot \sqrt{3k_x^2 - 3k_x + 1} \cdot \begin{bmatrix} v_{La} \\ v_{Lb} \\ v_{Lc} \end{bmatrix} \tag{36}$$

In (34), the $p_{\alpha\beta}$ and $q_{\alpha\beta}$ are the instantaneous active and reactive powers of the load in *α-β* plane, which include dc components $\bar{p}_{\alpha\beta}$, $\bar{q}_{\alpha\beta}$ and ac components $\tilde{p}_{\alpha\beta}$, $\tilde{q}_{\alpha\beta}$. $\bar{p}_{\alpha\beta}$ and $\bar{q}_{\alpha\beta}$ can be obtained through the low pass filters (LPFs), while $\tilde{p}_{\alpha\beta}$ and $\tilde{q}_{\alpha\beta}$ are calculated by subtracting $\bar{p}_{\alpha\beta}$ and $\bar{q}_{\alpha\beta}$ from $p_{\alpha\beta}$ and $q_{\alpha\beta}$, respectively. $p_{\alpha\beta}$ and $q_{\alpha\beta}$ can be obtained as,

$$\begin{bmatrix} p_{\alpha\beta} \\ q_{\alpha\beta} \end{bmatrix} = \begin{bmatrix} v_\alpha & v_\beta \\ -v_\beta & v_\alpha \end{bmatrix} \cdot \begin{bmatrix} i_\alpha \\ i_\beta \end{bmatrix} \tag{37}$$

In (37), the voltages ($v_\alpha$ and $v_\beta$) and currents ($i_\alpha$ and $i_\beta$) in the *α-β* plane can be transformed from *a-b–c* frames by,

$$\frac{d \max\left(\left|V_{inv1}\angle\theta_{V_{inv1}} + V_{inv2}\angle\theta_{V_{inv2}}\right|, \left|a^2 V_{inv1}\angle\theta_{V_{inv1}} + aV_{inv2}\angle\theta_{V_{inv2}}\right|, \left|aV_{inv1}\angle\theta_{V_{inv1}} + a^2 V_{inv2}\angle\theta_{V_{inv2}}\right|\right)}{dC} = 0 \tag{33}$$

$$\begin{bmatrix} v_\alpha \\ v_\beta \end{bmatrix} = \sqrt{\frac{2}{3}} \begin{bmatrix} 1 & -1/2 & -1/2 \\ 0 & \sqrt{3}/2 & -\sqrt{3}/2 \end{bmatrix} \cdot \begin{bmatrix} v_{La} \\ v_{Lb} \\ v_{Lc} \end{bmatrix} \tag{38}$$

$$\begin{bmatrix} i_\alpha \\ i_\beta \end{bmatrix} = \sqrt{\frac{2}{3}} \begin{bmatrix} 1 & -1/2 & -1/2 \\ 0 & \sqrt{3}/2 & -\sqrt{3}/2 \end{bmatrix} \cdot \begin{bmatrix} i_{La} \\ i_{Lb} \\ i_{Lc} \end{bmatrix} \tag{39}$$

where $v_{Lx}$ and $i_{Lx}$ are the load voltage and current signals. Finally, by comparing the compensating current $i_{cx}$ with its reference value $i_{cx}^*$ applying the pulse-width modulation (PWM) control method, the trigger signals for the active inverter part can be generated to control the insulated gate bipolar transistors (IGBTs). Based on the above analysis, the proposed overall control block of the CWTI-DSTATCOM is given in Fig. 10. In the proposed control, the parameters to be measured by the sensors are the load voltage $v_{Lx}$, the load current $i_{Lx}$, the compensation current $i_{cx}$, and the dc-link voltage $V_{dc}$. The implementation of this control scheme does not require additional sensors compared with the conventional WTI-STATCOM since the turn ratio $K_x$, and winding tap ratio $k_x$ are settled and given in advance.

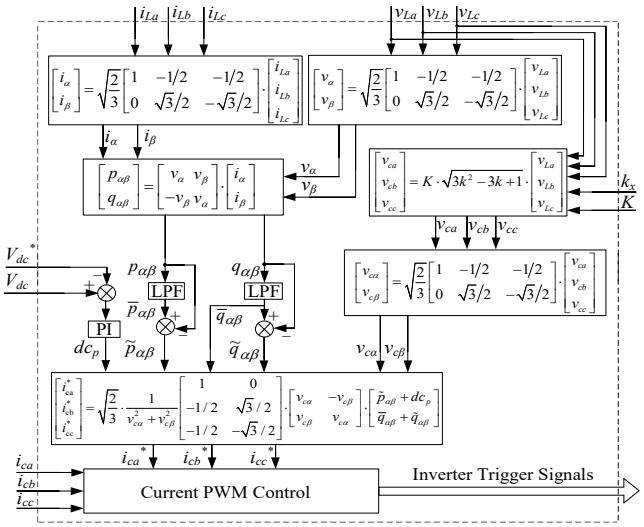


Fig. 10. Overall control block of the CWTI-DSTATCOM.

## V. Simulation Results

In this section, the simulation case studies are provided to verify: a) the proposed CWTI-DSTATCOM can compensate the reactive and unbalanced load under lower dc-link voltage and VSI power rating in comparison with the WTI-DSTATCOM; b) the proposed *LC* design method of CWTI-DSTATCOM for the unbalanced load can further decrease the required dc-link voltage and VSI power rating compared with the conventional balanced *LC* design method. The simulation parameters are listed in Table IV.

Table V summarizes the compensating performances of the WTI-DSTATCOM and proposed CWTI-DSTATCOM.

TABLE IV
Simulation/ Experimental System Parameters

| | Parameters | | Physical values |
|---|---|---|---|
| System | $V_{sx}$, $V_{Lx}$, $k_x$ | | 10kV/√3, 220V, 0.5 |
| WTI-DSTATCOM | $L$ | | 10 mF |
| CWTI-DSTATCOM | Conventional design | $L$, $C$ | 10 mF, 25 μF |
| | Proposed design | $L$, $C$ | 10 mF, 30.6 μF |
| Load | $R_{La}$, $L_{La}$, $R_{Lb}$, $L_{Lb}$, $R_{Lc}$, $L_{Lc}$ | | 0.4 Ω, 1 mF, 0.25 Ω, 0.5 mF, 0.4 Ω, 1 mF |

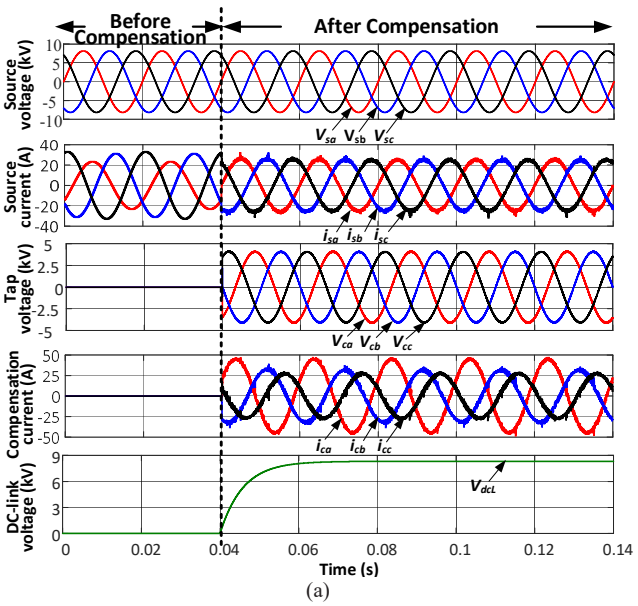


(a)

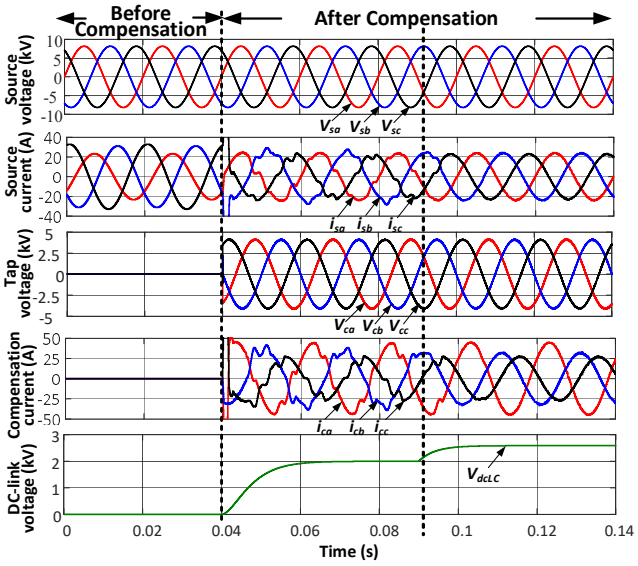


(b)

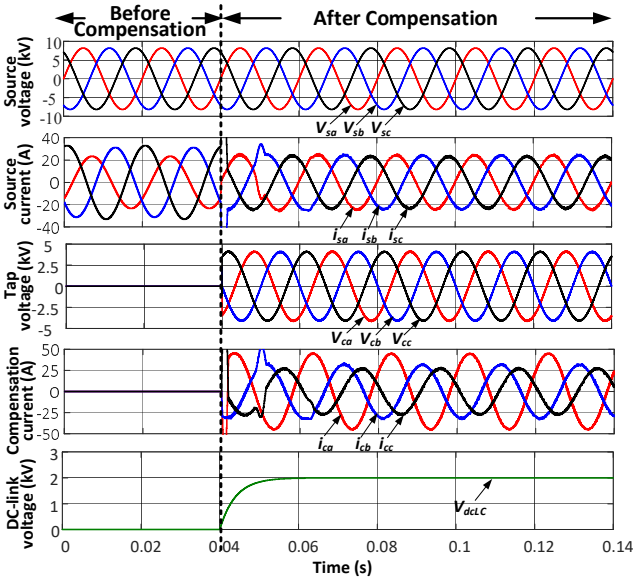


(c)

Fig. 11. Dynamic compensating performance by applying (a) WTI-DSTATCOM; (b) CWTI-DSTATCOM with conventional *LC* design; (c) CWTI-DSTATCOM with proposed *LC* design.

TABLE V
SIMULATION RESULTS WITH ε=0.3 WHEN $V_{sx}$=10KV, $K_x$ = 0.5

| Situations | | $V_{dc}$ (V) | Phase | $I_{Sx}$ (A) | $Q_{Sx}$ (kVAR) | $PF_{Sx}$ | THD $i_{Sx}$(%) | $\varepsilon$ (%) | Loss (kW) |
|---|---|---|---|---|---|---|---|---|---|
| Before comp. | | – | A | 23.4∠-38.4 | 59.0 | 0.79 | 0 | 30 | – |
| | | | B | 31.2∠-145.7 | 54.8 | 0.90 | 0 | | |
| | | | C | 33∠76.9 | 91.7 | 0.73 | 0 | | |
| Coupling $L$=10mH (WTI-DSTATCOM) | | 8300 | A | 25.2∠−0.4 | 0.5 | 1.00 | 4.9 | 0.2 | 5.84 |
| | | | B | 25.1∠−120.3 | 0.4 | 1.00 | 4.9 | | |
| | | | C | 25.2∠119.8 | 0.04 | 1.00 | 4.8 | | |
| Proposed topology | Conventional design with $L$=10mH, $C$=25μF | 2000 | A | 23.5∠5.6 | -9.8 | 0.994 | 9.7 | 11.4 | – |
| | | | B | 26∠−123.9 | 6.8 | 0.998 | 8.2 | | |
| | | | C | 21.2∠115.1 | 7.2 | 0.996 | 11.3 | | |
| | | 2800 | A | 23.6∠0.99 | -1.9 | 1.00 | 1.7 | 2.7 | 2.57 |
| | | | B | 23.9∠−121.5 | 2.2 | 1.00 | 2.0 | | |
| | | | C | 23∠119.5 | 4.9 | 1.00 | 1.1 | | |
| | Unbalanced design with $L$=10mH, $C$=30.6μF | 2000 | A | 24.3∠0.74 | -1.6 | 1.00 | 2.4 | 1.6 | 2.03 |
| | | | B | 24.3∠−121.3 | 1.9 | 1.00 | 2.6 | | |
| | | | C | 24.1∠119.7 | 0.2 | 1.00 | 2.9 | | |
| | | 1950 | A | 24.1∠2.6 | -4.7 | 1.00 | 8.1 | 6 | 2.01 |
| | | | B | 25.2∠−122.5 | 3.7 | 1.00 | 2.1 | | |
| | | | C | 22.7∠117.5 | 1.4 | 1.00 | 8.4 | | |
| | | 1900 | A | 18.5∠−0.8 | 0.9 | 0.997 | 23.8 | 17.6 | – |
| | | | B | 25.2∠−126.4 | 11.1 | 0.995 | 32.3 | | |
| | | | C | 20.8∠99.9 | 29 | 0.938 | 31.6 | | |

TABLE VI
DC-LINK VOLTAGE AND RATING COMPARISONS BETWEEN THEORY AND SIMULATION

| | Theory value (V) | Simulation value (V) | Ratio | Theory value | Simulation value |
|---|---|---|---|---|---|
| $V_{dcL\_bal}$ | 8000 | – | $R_{LC\_bal}/R_{L\_bal}$ | 0.12 | – |
| $V_{dcLC\_bal}$ | 930 | – | $R_{L\_unbal}/R_{L\_bal}$ | 1.35 | 1.35 |
| $V_{dcL\_unbal}$ | 8279 | 8300 | $R_{LC\_unbal}/R_{L\_unbal}$ | 0.33 | 0.34 |
| $V_{dcLC\_unbal}$ | 2772 | 2800 | $R_{LC\_unbal}/R_{LC\_bal}$ | 3.87 | 3.63 |

Fig. 11 shows the dynamic performance of different cases before and after compensation. It can be seen that the WTI-DSTATCOM and CWTI-DSTATCOM both can well operate under IEEE standard [34], with the source current $\varepsilon$ less than 3%, source side PF equal to 1, and total harmonic distortions ($THD_{iSx}$) less than 5%. The required dc-link voltage of CWTI-DSTATCOM is 2800V which is lower than 8300V of WTI-DSTATCOM. To verify the dc-link voltage is the factor to affect the compensating performance, dc-link voltage 2000V is given for the CWTI-DSTATCOM with conventional $LC$ design. The dc-link voltage 2000V is not enough for compensation so that $PF_{Sx}$ =0.994, $THD_{iSx}$ (%) = 11.3 (the worst value from 3 phases), and $\varepsilon$ =11.4%. When the dc-link voltage is 2800V, the performance is better with $PF_{Sx}$ =1, $THD_{iSx}$ (%) = 2.0 (the worst value from 3 phases), and $\varepsilon$ =2.7%. With the optimal $LC$ design, the proposed CWTI-DSTATCOM can also achieve the compensation requirements with only 2000V dc-link voltage, which is 3.15 times smaller than the WTI-DSTATCOM. The compensating performances of three different dc-link voltages are also compared in Table V, which are below point B (1900V), point B (1950V), and above point B (2000V) of Fig. 9. These verify that the calculated theoretical 1950 V is the minimum dc-link voltage to achieve the acceptable compensating performance.

Under full compensation, the compensation current $I_{c1}$=33.6 ∠ 90, $I_{c2}$=11.6 ∠ 95.6, and $\varepsilon$ is about 0.3. The theoretical and simulated values comparisons of dc-link are shown in Table VI. The power rating ratios of $R_{LC}/R_L$ and $R_{unbal}/R_{bal}$ in simulation and in theory are almost the same, which verifies the feasibility of power rating calculation formulas in Section II-D. Under this unbalanced load, for CWTI-DSTATCOM based on conventional balanced $LC$ design, its dc-link voltage is reduced by 66.8%, and its VSI power rating is about 1/3 of that of WTI-DSTATCOM. With the proposed unbalanced $LC$ design, its dc-link voltage is reduced approximately by 76.4%, and its VSI power rating is about 1/4.

## VI. EXPERIMENTAL RESULTS

In this section, the proposed CWTI-DSTATCOM and $LC$ filter design method for unbalance load have been verified in a real-time digital simulator (RTDS) hardware-in-the-loop (HIL) system, as shown in Fig. 12. The output $v_{sx}$, $i_{Sx}$, $v_{cx}$, $i_{cx}$, $V_{dc}$ signals are collected by DSP TMS320F28335. The DSP can calculate reference compensation current $i_{cx}^*$. Then the RTDS can control the IGBTS models to generate compensating current $i_{cx}$. All experimental waveforms are recorded by the Yokogawa DL850 oscilloscope in real-time. The load and system parameters in the experiment are the same as in the simulation. The experimental dynamic performance and results comparisons are shown in Fig. 13 and Table VII. After compensation of WTI-DSTATCOM with 8300V dc-link voltage, balanced source current, PF=1, and small source current ripple can all achieve. For the CWTI-DSTATCOM with 25$\mu$F capacitance, $V_{dcLC}$ must be increased from 2000V to 2800V to achieve the above satisfactory compensation for this unbalanced load. For the WTI-DSTATCOM with 30.6$\mu$F capacitance, the

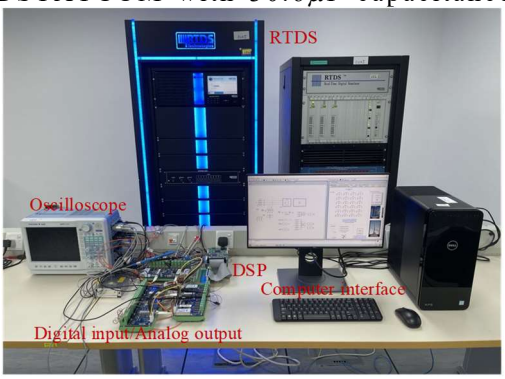


Fig. 12. Physical layout of experimental test environment.

TABLE VII
EXPERIMENTAL RESULTS WITH ε=0.3 WHEN $V_{sx}$=10KV, $K_x$ = 0.5

| Situations | | $V_{dc}$ (V) | Phase | $I_{iSx}$ (A) | $Q_{Sx}$ (kVAR) | $PF_{Sx}$ | $THD_{iSx}$ (%) | $\varepsilon$ (%) | Loss (kW) |
|---|---|---|---|---|---|---|---|---|---|
| Before comp. | | – | A | 23.4∠-38.4 | 59.0 | 0.79 | 0 | 30 | – |
| | | | B | 31.2∠-145.7 | 54.8 | 0.90 | 0 | | |
| | | | C | 33∠76.9 | 91.7 | 0.73 | 0 | | |
| Coupling $L$=10mH (WTI-DSTATCOM) | | 8300 | A | 24.9∠−0.5 | 0.4 | 1.00 | 3.5 | 1.5 | 5.80 |
| | | | B | 25.2∠−120.5 | 0.3 | 1.00 | 4.1 | | |
| | | | C | 24.9∠119.6 | 0.2 | 1.00 | 3.9 | | |
| Proposed topology | Conventional design with $L$=10mH, $C$=25μF | 2000 | A | 21.5∠5.6 | 8.0 | 0.995 | 7.6 | 12 | – |
| | | | B | 25.4∠−123.9 | 6.8 | 0.998 | 10.3 | | |
| | | | C | 23.2∠115.1 | -8.1 | 0.997 | 4.2 | | |
| | | 2800 | A | 23.9∠0.89 | -0.9 | 1.00 | 2.5 | 2.6 | 2.61 |
| | | | B | 24.2∠−121.5 | 0.4 | 1.00 | 2.6 | | |
| | | | C | 24.1∠119.5 | 0.2 | 1.00 | 2.4 | | |
| | Unbalanced design with $L$=10mH, $C$=30.6μF | 2000 | A | 24.2∠0.56 | -0.8 | 1.00 | 2.4 | 1.7 | 2.05 |
| | | | B | 24.3∠−121.5 | 0.4 | 1.00 | 2.6 | | |
| | | | C | 24.2∠119.6 | 0.5 | 1.00 | 2.4 | | |

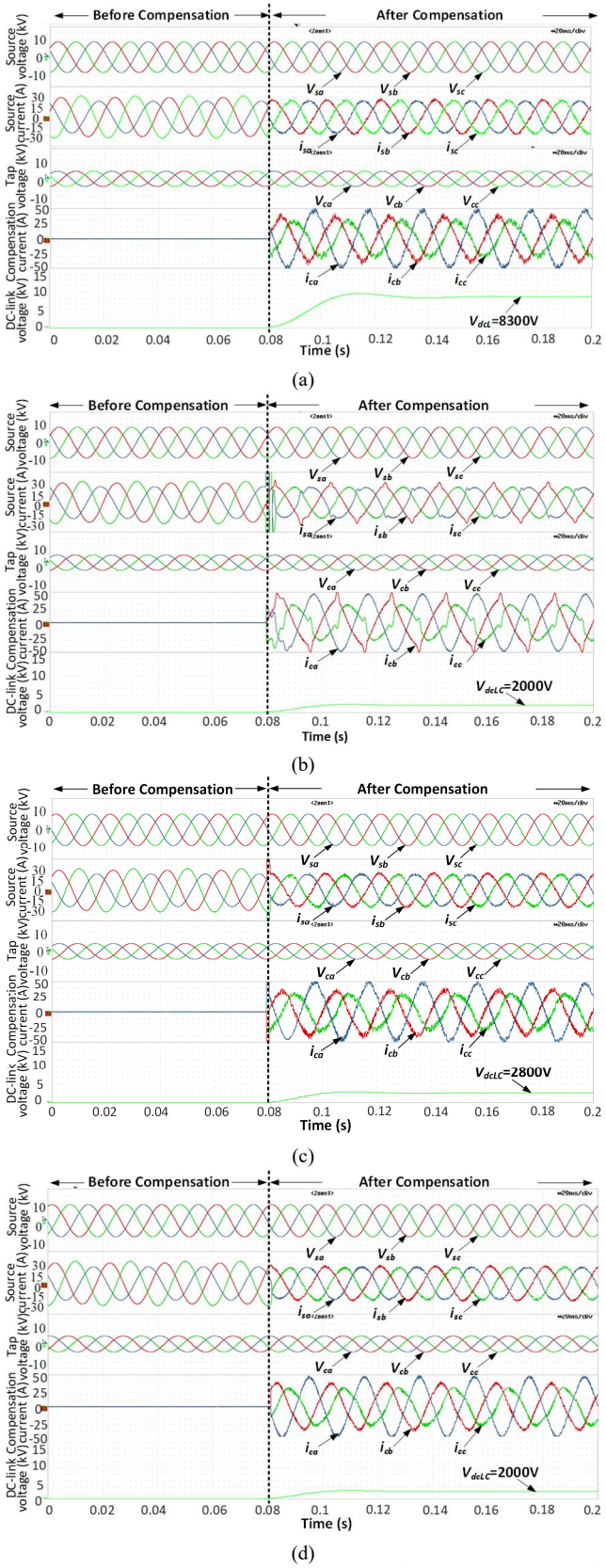


Fig. 13. Experimental performance before and after compensation by applying (a) WTI-DSTATCOM at $V_{dcL}$= 8300V; (b) CWTI-DSTATCOM with conventional *LC* design at $V_{dcLC}$= 2000V; (c) CWTI-DSTATCOM with proposed *LC* design at $V_{dcLC}$= 2800V; (d) CWTI-DSTATCOM with proposed *LC* design with $V_{dcLC}$= 2000V.

compensation results reflect that it can well operate in balancing the load current and compensating reactive power at a 2000V dc-link voltage. All in all, compared with conventional topology and design method, the CWTI-DSTATCOM with proposed *LC* design method can provide a much lower dc-link voltage and significantly reduce the VSI power rating requirement.

## VII. Conclusions

In this paper, a CWTI-DSTATCOM equipped in the smart substation is proposed for cost-effective balanced and unbalanced compensation. The modelings of the CWTI-DSTATCOM based on the symmetrical components are expressed to reveal the dc-link voltage and VSI power rating reduction mechanism, which are further ensured based on an optimal *LC* design. Its corresponding control strategy for load compensation is proposed to coordinate the transformer taps and the active inverter. Finally, it can be concluded from the simulation and experimental results that 1) with the *LC*-coupling, the required dc-link voltage of CWTI-DSTATCOM can be reduced significantly; 2) under balanced situations, the inverter rating of CWTI-DSTATCOM is only 12% of WTI-DSTATCOM. Under an unbalanced situation at 0.3 unbalance coefficient, the VSI rating of CWTI-DSTATCOM by conventional design is about 1/3 of the WTI-DSTATCOM. Moreover, with the proposed unbalanced design, CWTI-DSTATCOM is about 1/4 VSI rating of WTI-DSTATCOM; 3) the VSI power rating ratios between CWTI-DSTATCOM and WTI-DSTATCOM are mathematically formulated for balance and unbalance operations.

## Appendix

### A. Cost Reduction Analysis

The costs of WTI-DSTATCOM and CWTI-DSTATCOM structures can be approximately calculated as (40) and (41).

$$\mathrm{Cost}_{WTI-DSTATCOM} \approx \mathrm{Cost}_{STATCOM} + \mathrm{Cost}_{L} \tag{40}$$

$$\mathrm{Cost}_{CWTI-DSTATCOM} \approx \mathrm{R}_{tot} \cdot \mathrm{Cost}_{STATCOM} + (1-\mathrm{R}_{tot}) \cdot \mathrm{Cost}_{C} + \mathrm{Cost}_{L} \tag{41}$$

where $\mathrm{Cost}_{STATCOM}$ and $\mathrm{Cost}_{L}$ are the costs of STATCOM and coupling *L* respectively for WTI-DSTATCOM; $\mathrm{R}_{tot}$ (%) is the VSI rating ratio between CWTI-STATCOM and WTI-STATCOM. According to the rating modeling part in section II, the $\mathrm{R}_{tot}$ is 12% for balanced load, and $\mathrm{R}_{tot}$ is 1/3 for unbalanced load with $\varepsilon$=0.3. The costs $\mathrm{Cost}_{L}$ of coupling *L* are the same for CWTI-STATCOM and WTI-STATCOM, which can be ignored in the cost comparison of CWTI-STATCOM and WTI-STATCOM. According to investment costs of the fixed capacitor and STATCOM in the typical medium voltage level applications [35], the cost comparison of the proposed CWTI-DSTATCOM and WTI-STATCOM for $\varepsilon$=0 and $\varepsilon$=0.3 loads can be shown in Fig. 14. It can be observed that the proposed CWTI-DSTATCOM is more cost-effective than the traditional WTI-DSTATCOM.

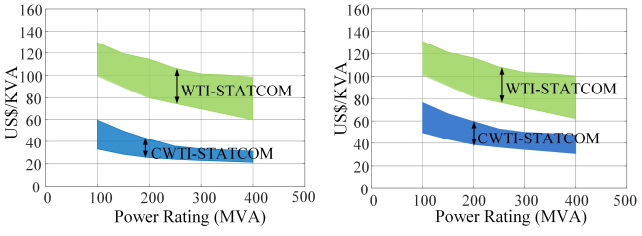


Fig. 14. Investment costs of CWTI-DSTATCOM for the (a) balanced load; (b) unbalanced load.

### B. Power Loss Case Study

Less dc-link voltage means less power loss. According to the power loss studies [36], [37], the a) switching loss and b) component conduction loss contribute to the major power loss of the proposed structure.

*a) Switching Loss*

The switching loss is influenced by the collector-emitter voltage and current of each IGBT, which can be classified as turn-on and turn-off losses. (42) is the total turn-on and turn-off power losses.

$$P_{loss(sw)} = V_{dc} I_{loss} = V_{dc} I_{CM} f_{sw} \left( \frac{1}{8} t_{on} \frac{I_{CM}}{I_{CN}} + t_{off} \left( \frac{1}{3\pi} + \frac{1}{24} \frac{I_{CM}}{I_{CN}} \right) \right) \quad (42)$$

where $V_{dc}$, $I_{CM}$, $I_{CN}$, $t_{on}$, $t_{off}$, and $f_{sw}$ are the dc-link voltage, maximum collector current, rated collector current, rated rise time, rated fall time, and switching frequency, respectively. Thus, the higher $V_{dc}$ of the WTI-STATCOM and CWTI-STATCOM, the higher the switching losses are obtained and vice versa.

*b) Component Conduction Loss*

For WTI-DSTATCOM and CWTI-DSTATCOM, the component conduction power losses can be expressed as (43) and (44).

$$P_{\text{loss}(L)} = ESR_L \cdot I_{cx}^2 \quad (43)$$

$$P_{\text{loss}(LC)} = ESR_L \cdot I_{cx}^2 + ESR_C \cdot I_{cx}^2 \quad (44)$$

where $ESR_L$ (=0.18Ω) and $ESR_C$ (=0.33Ω) are equivalent series resistance of coupling inductor $L$, coupling capacitor $C$.

Based on the above analysis, the total power losses of WTI-STATCOM and CWTI-STATCOM are shown in Table V and Table VII. It shows that the total power loss of the proposed CWTI-STATCOM is much lower than that of WTI-STATCOM.

## REFERENCES


[1] M. S. Golsorkhi, D. J. Hill, and M. Baharizadeh, "A secondary control method for voltage unbalance compensation and accurate load sharing in networked microgrids," *IEEE Trans. Smart Grid*, vol. 12, no. 4, pp. 2822–2833, Jul. 2021.

[2] R. Kalpana, K. S. Chethana, S. P. P, and B. Singh, "Power quality enhancement using current injection technique in a zigzag configured autotransformer-based 12-pulse rectifier," *IEEE Trans. Ind. Appl.*, vol. 54, no. 5, pp. 5267–5277, Sep./Oct. 2018.

[3] K. K. Prasad, H. Myneni, and G. S. Kumar, "Power quality improvement and PV power injection by DSTATCOM with variable DC link voltage control from RSC-MLC," *IEEE Trans. Sustain. Energy*, vol. 10, no. 2, pp. 876–885, Apr. 2019.

[4] M. N. Slepchenkov, K. M. Smedley, and J. Wen, "Hexagram-converter-based STATCOM for voltage support in fixed-speed wind turbine generation systems," *IEEE Trans. Ind. Electron*., vol. 58, no. 4, pp. 1120–1131, Apr. 2011.

[5] G. Levitin, A. Kalyuzhny, A. Shenkman, and M. Chertkov, "Optimal capacitor allocation in distribution systems using a genetic algorithm and a fast energy loss computation technique," *IEEE Trans. Power Del*., vol. 15, no. 2, pp. 623–628, Apr. 2000.

[6] Y. Li, T. K. Saha, O. Krause, Y. Cao, and C. Rehtanz, "An inductively active filtering method for power-quality improvement of distribution networks with nonlinear loads," *IEEE Trans. Power Del.,* vol. 28, no. 4, pp. 2465–2473, Oct. 2013.

[7] S. X. Chen, Y. S. Foo. Eddy, H. B. Gooi, M. Q. Wang, and S. F. Lu, "A centralized reactive power compensation system for LV distribution networks," *IEEE Trans. Power Syst.*, vol. 30, no. 1, pp. 274–284, Jan. 2015.

[8] Q. Liu, Y. Li, S. Hu and L. Luo, "A transformer integrated filtering system for power quality improvement of industrial DC supply system," *IEEE Trans. Ind. Electron*., vol. 67, no. 5, pp. 3329-3339, May 2020.

[9] O. P. Mahela and A. G. Shaik, "A review of distribution static compensator," *Renew. Sustain. Energy Rev*., vol. 50, pp. 531–546, May. 2015.

[10] B. Singh, P. Jayaprakash, D. P. Kothari, A. Chandra and K. Al Haddad, "Comprehensive study of DSTATCOM configurations," *IEEE Trans. Ind. Informat.*, vol. 10, no. 2, pp. 854-870, May 2014.

[11] C. O. Gercek and M. Ermis, "Elimination of coupling transformer core saturation in cascaded multilevel converter-based T-STATCOM systems," *IEEE Trans. Power Electron.*, vol. 29, no. 12, pp. 6796–6809, Dec. 2014.

[12] M. Vijeh, M. Rezanejad, E. Samadaei and K. Bertilsson, "A general review of multilevel inverters based on main submodules: structural point of view," *IEEE Trans. Power Electron.*, vol. 34, no. 10, pp. 9479-9502, Oct. 2019.

[13] J. Falck, C. Felgemacher, A. Rojko, M. Liserre and P. Zacharias, "Reliability of power electronic systems: An industry perspective," *IEEE Ind. Electron. Mag*., vol. 12, no. 2, pp. 24-35, Jun. 2018.

[14] S. J. Hu *et al*., "A new integrated hybrid power quality control system for electrical railway," *IEEE Trans. Ind. Electron.*, vol. 62, no. 10, pp. 6222–6232, Oct. 2015

[15] C. Wang, X. Yin, Z. Zhang, and M. Wen, "A novel compensation technology of static synchronous compensator integrated with distribution transformer," *IEEE Trans. Power Del.*, vol. 28, no. 2, pp. 1032–1039, Apr. 2013.

[16] Y. Li, L. Luo, C. Rehtanz, S. Rüberg, and D. Yang, "An industrial DC power supply system based on an inductive filtering method," *IEEE Trans. Ind. Electron.*, vol. 59, no. 2, pp. 714–722, Feb. 2012.

[17] Y. Li *et al*., "A virtual impedance comprehensive control strategy for the controllably inductive power filtering system," *IEEE Trans. Power Electron.*, vol. 32, no. 2, pp. 920–926, Feb. 2017.

[18] Q. Liu, Y. Li, S. Hu, and L. Luo, "Power quality improvement using controllable inductive power filtering method for industrial DC supply system," *Control Eng. Pract.,* vol. 83, pp. 1–10, Feb. 2019.

[19] Y. Li, T. K. Saha, O. Krause, Y. Cao and C. Rehtanz, "An inductively active filtering method for power-quality improvement of distribution networks with nonlinear loads," *IEEE Trans. Power Del.*, vol. 28, no. 4, pp. 2465-2473, Oct. 2013.

[20] Q. Liu, Y. Li, L. Luo, Y. Peng, and Y. Cao, "Power quality management of PV power plant with transformer integrated filtering method," *IEEE Trans. Power Del.*, vol. 34, no. 3, pp. 941–949, Jun. 2019.

[21] Chi-Seng Lam and Man-Chung Wong, "Investigation of a novel capacitive-coupled STATCOM: modeling and simulation." *IEEE 43rd UPEC 2008*, Sept. 2008.

[22] Chi-Seng Lam, Fan Ng, Man-Chung Wong, "Control scheme of a novel capacitive-coupled STATCOM," *IEEE 43rd UPEC 2008,* Sept. 2008.

[23] L. Wang, C. S. Lam, and M. C. Wong, "A hybrid STATCOM with wide compensation range and low dc-link voltage," *IEEE Trans. Ind. Electron.,* vol. 63, no. 6, pp. 3333–3343, Jun. 2016.

[24] Y. Li, F. Liu, T. K. Saha, O. Krause, and Y. Cao, "Hybrid inductive and active filtering method for damping harmonic resonance in distribution network with non-linear loads," *IET Power Electron*., vol. 8, no. 9, pp. 1616–1624, Sep. 2015.

[25] Y. Li *et al*., "A controllably inductive filtering method with transformer integrated linear reactor for power quality improvement of shipboard power system," *IEEE Trans. Power Del.*, vol. 32, no. 4, pp. 1817–1827, Aug. 2017.

[26] Q. Liu, Y. Li, S. Hu and L. Luo, "A transformer integrated filtering system for power quality improvement of industrial DC supply system," *IEEE Trans. Ind. Electron.,* vol. 67, no. 5, pp. 3329-3339, May 2020.

[27] B. Xie, Z. Zhang, S. Hu, Y. Li, L. Luo, and S. Sun, "YN/VD connected balance transformer-based electrical railway negative sequence current compensation system with passive control scheme," *IET Power Electronics*, vol. 9, no. 10, pp. 2044–2051, Aug. 2016.

[28] Z. Zhang *et al*., "Reactive power compensation and negative-sequence current suppression system for electrical railways with YNvd-connected balance transformer—Part I: Theoretical analysis," *IEEE Trans. Power Electron.*, vol. 33, no. 1, pp. 272–282, Jan. 2018.

[29] S. Hu *et al*., "A Y-D multifunction balance transformer-based power quality control system for single-phase power supply system," *IEEE Trans. Ind. Appl.,* vol. 52, no. 2, pp. 1270–1279, Mar./Apr. 2016.

[30] E. Lei, X. Yin, Z. Zhang, and Y. Chen, "An improved transformer winding tap injection DSTATCOM topology for medium-voltage reactive power compensation," *IEEE Trans. Power Electron*., vol. 33, no. 3, pp. 2113–2126, Mar. 2018.

[31] Y. Chen *et al.*, "Passivity-based control of cascaded multilevel converter based D-STATCOM integrated with distribution transformer," *Elect. Power Syst. Res.*, vol. 154, pp. 1–12, 2018.
[32] Z. Wang, X. Yin, Y. Chen, J. Lai, L. Li, and Z. Qi, "DSTATCOM integrated with Y-y connection transformer for reactive power compensation," *Int. J. Electr. Power Energy Syst.*, vol. 117, p. 105721, May 2020.
[33] M.-C. Wong, Y. Pang, Z. Xiang, L. Wang, and C.-S. Lam, "Assessment of active and hybrid power filters under space vector modulation," *IEEE Trans. Power Electron., vol*. 36, no. 3, pp. 2947–2963, Mar. 2021.
[34] *IEEE recommended practices and requirements for harmonic control in electrical power systems*, IEEE standard 519-2014, 2014.
[35] L. M. Tolbert, *et al.*, "Power electronics for distributed energy systems and transmission and distribution applications: Assessing the technical needs for utility applications," Oak Ridge Nat. Lab., Oak Ridge, TN, USA, Tech. Rep. ORNL/TM-2005/230, Dec. 2005.
[36] E. Serban; C. Pondiche; and M. Ordonez, "Modulation effects on power-loss and leakage current in three-phase solar inverters," *IEEE Trans. Energy Convers.*, vol. 34, no. 1, pp. 339-350, Jan. 2019.
[37] L. Wang, C.-S. Lam, and M.-C. Wong, "Minimizing inverter capacity design and comparative performance evaluation of SVC-coupling hybrid active power filters," *IEEE Trans. Power Electron.*, vol. 34, no. 2, pp. 1227–1242, Feb. 2019.

**Ziyi Bai** received the B.Sc. degree in electrical engineering from Hainan University, Haikou, China, in 2016, and the M.Sc. degree in electrical engineering from Hunan University, Changsha, China, in 2019. She is currently pursuing the Ph.D. degree in electrical and computer engineering with the State Key Laboratory of Internet of Things for Smart City, University of Macau, Macau, China. Her research interests include power quality, smart grid, renewable energy, and distributed generation.

**Ying Pang** (S'19) received the B.Sc. degree in electrical engineering from Southwest Jiaotong University, Chengdu, China, in 2015, and the M.Sc. degree in electrical and computer engineering from the University of Macau, Macao, in 2018, where he is currently pursuing the Ph.D. degree in electrical and computer engineering with the State Key Laboratory of Internet of Things for Smart City. His research interests include power filter, smart grid, renewable energy, and distributed generation.

**Zeng Xiang** (Member, IEEE) received the B.Sc. degree in Electrical Engineering and Automation from Tianjin University of Science & Technology, in 2009, Tianjin, China. He received his M.Sc. degree in Electronic Engineering from Hunan University, in 2012, Changsha, China.
From 2012 to 2015, he was an R&D engineer in Zhuhai Wanlida Electrical Automation Co., Ltd., Zhuhai, China.
He is currently working toward the Ph.D. degree in Electrical and computer engineering with State Key Laboratory of Internet of Things for Smart City, University of Macau, Macau. His research interests include high-performance converters for microgrids, power quality, and distributed power generation system.

**Chi-Kong Wong** (Member, IEEE) received the B.Sc. and M.Sc. degrees in electrical and electronics engineering from the University of Macau (UM), Macao, China, in 1993 and 1997, respectively, and the Ph.D. degree in electrical engineering from Tsinghua University, Beijing, China, in 2007.

Since 1993, he has been a Teaching Assistant with the Faculty of Science and Technology, UM, where he was promoted as a Lecturer and an Assistant Professor in 1997 and 2008, respectively. His current research interests include power electronics' controllers, power system analysis, power quality compensators, and renewable energy.

Dr. Wong has been an IEEE Student Branch Officer since 1997. He is currently the Vice-Chair of IEEE Macau Section and the Committee Member of IEEE Macau PES/PELS Joint Chapter.

**Lei Wang** (SM'20) received the B.Sc. degree in Electrical and Electronics Engineering from University of Macau (UM), Macao SAR, P. R. China, in 2011, M.Sc. degree in Electronics Engineering from Hong Kong University of Science and Technology (HKUST), Hong Kong SAR, P. R. China, in 2012. and Ph.D. degree in Electrical and Computer Engineering from UM, Macao SAR, P. R. China, in 2017.

He was a postdoctoral fellow in the Power Electronics Laboratory of UM from Jan. 2017 to Feb. 2019. He was a visiting fellow in department of electrical and computer engineering, University of Auckland, from Feb. 2019 to Aug. 2019. In 2019, he joined College of Electrical and Information Engineering, Hunan University, Changsha, China, where he is currently a Full Professor.

He has authored 1 Springer books, 1 Elsevier book chapter, 5 patents (U.S.A and China) and over 30 journal and conference papers. Dr. Wang received the champion award in the "Schneider Electric Energy Efficiency Cup", Hong Kong, 2011, Macao Science and Technology R&D Award for Postgraduates (Ph.D) in 2018.

**Chi-Seng Lam** (Senior Member, IEEE) received the Ph.D. degree in electrical and electronics engineering from the University of Macau (UM), Macao, China, in 2012. He completed the Clare Hall Study Programme at the University of Cambridge, Cambridge, U.K., in 2019. From 2006 to 2009, he was an Electrical and Mechanical Engineer with UM.

From 2009 to 2012, he simultaneously worked as a Laboratory Technician at UM, and pursued his Ph.D. degree in part-time at UM. In 2013, he was a Post-Doctoral Fellow with The Hong Kong Polytechnic University, Hong Kong, China. He is currently an Associate Professor with the State Key Laboratory of Analog and Mixed-Signal VLSI and the Institute of Microelectronics, UM, and also with the Department of Electrical and Computer Engineering, Faculty of Science and Technology, UM. He has coauthored or co-edited four books and more than 110 technical journals and conference papers. He holds four U.S. and two Chinese patents. His research interests include power quality compensators, renewable energy generation, integrated power electronics controllers, power management integrated circuits, and wireless power transfer.

Dr. Lam serves/served as a member for the Organizing Committee or Technical Program Committee of IEEE international conferences, including IECON 2020, IECON 2019, ASSCC 2019, APPEEC 2019, IECON 2018, IESES 2018, ASP-DAC 2016, and TENCON 2015. He was a recipient or corecipient of the IEEE PES Chapter Outstanding Engineer Award in 2016, the Best Track Paper Award of APPEEC 2019, the Best Paper Award of ICTA 2019, the Merit Paper Award of the 3rd RIUPEEEC Conference in 2005, the Macao Science and Technology Invention Award (Second Class and Third Class) and the Research and Development Award for Postgraduates (Ph.D.) in 2018, 2014, and 2012, respectively. He was the Vice-Chair of the IEEE Macau Section from 2016 to 2020 and the Chair of the IEEE Macau CAS Chapter from 2017 to 2018. He is currently the Chair of the IEEE Macau IES Chapter and the Power Quality Subcommittee Chair of the IEEE IES Technical Committee on Power Electronics. He serves as an Associate Editor for IEEE Transactions on Industrial Electronics and IEEE Access, and a Guest Editor for the IEEE Transactions on Circuits and Systems II: Express Briefs and the IET Power Electronics in 2020.

**Man-Chung Wong** (SM'06) received the B.Sc. and M.Sc. degrees in Electrical and Electronics Engineering from University of Macau (UM), Macao, China, and got his Ph. D. degree from Department of Electrical Engineering, Tsinghua University, Beijing, P. R. China.

He is currently a professor in the Department of Electrical and Computer Engineering, University of Macau and he was a visiting fellow in Cambridge University, now he is affiliated with State Key Laboratory of Internet of Thing Smart City and Sate Key Laboratory of Analog and Mixed Signal VLSI, University of Macau.

He published four books and more than 150 technical journals and conference papers. He holds four U.S. patent and 8 Chinese patents. His research interests include integrated power electronics controllers, power electronics converters, power quality compensators, renewable energy, wireless power transfer and smart grid.

Prof. Wong was a recipient of Macao Science and Technology Invention Awards (2nd Class at 2018, 3rd Class at 2014 and 2012 respectively) and Yong Scientist Award from Insituto Internacional De Macau at 2000, Young Scholar Award form University of Macau at 2001, Second Prize of 2003 Tsinghua University Excellent Doctor Thesis Award. He was IEEE TENCON Macao 2015 General Chair and IEEE APPEEC Macao 2019 General Chair. He was Chair of IEEE Macau Section at 2014- 2015, he is currently the Chair of IEEE Macau PES/PELS Joint Chapter and IEEE Region 10 Power and Energy Society North Representative since 2015. Since 2017, he is department head of Electrical and Computer Engineering, FST, University of Macau.